Catalysis Science & Technology

Accepted Manuscript

This is an *Accepted Manuscript*, which has been through the Royal Society of Chemistry peer review process and has been accepted for publication.

Accepted Manuscripts are published online shortly after acceptance, before technical editing, formatting and proof reading. Using this free service, authors can make their results available to the community, in citable form, before we publish the edited article. We will replace this *Accepted Manuscript* with the edited and formatted *Advance Article* as soon as it is available.

You can find more information about *Accepted Manuscripts* in the Information for Authors.

Please note that technical editing may introduce minor changes to the text and/or graphics, which may alter content. The journal's standard Terms & Conditions and the Ethical guidelines still apply. In no event shall the Royal Society of Chemistry be held responsible for any errors or omissions in this *Accepted Manuscript* or any consequences arising from the use of any information it contains.

ROYAL SOCIETY OF CHEMISTRY

www.rsc.org/catalysis

KNO_3 supported on three-dimensionally ordered macroporous $La_{0.8}Ce_{0.2}Mn_{1-x}Fe_xO_3$ for soot removal

Nengjie Feng, Jie Meng, Yang Wu, Chong Chen, Lei Wang, Lu Gao, Hui Wan*, Guofeng Guan*

State Key Laboratory of Materials-Oriented Chemical Engineering, College of Chemical Engineering, Nanjing Tech University, Nanjing 210009, PR China

*Corresponding author, telephone: +86-25-83587198. E-mail: wanhui@njtech.edu.cn; guangf@njtech.edu.cn

Abstract:

Three-dimensionally ordered macroporous (3DOM) $La_{0.8}Ce_{0.2}Mn_{1-x}Fe_xO_3$ perovskites were successfully prepared by colloidal crystal template method and KNO_3-supported 3DOM $La_{0.8}Ce_{0.2}Mn_{1-x}Fe_xO_3$ catalysts were prepared by wetness impregnation method. Physicochemical properties of these catalysts were characterized by XRD, FT-IR, FESEM, TEM, BET, H_2-TPR, O_2-TPD, and XPS techniques and their catalytic performances were evaluated by the soot combustion. All these perovskites possessed well-ordered 3DOM structure, and KNO_3 was highly dispersed on the skeleton of supporters without changing the morphology and crystal structure of the perovskites. 3DOM structure provided more contact areas between catalyst and soot. Besides, partial replacement of Mn by Fe into the perovskites increased the surface areas and reducibilities. The introduction of K ions increased the amount of active oxygen species in the catalysts, which could accelerate soot combustion at the low temperature. On the other hand, the NO_3^- species brought by KNO_3 were beneficial to

Catalysis Science & Technology Accepted Manuscript

the reaction at the high temperature. Among all the samples, the 3DOM $K/La_{0.8}Ce_{0.2}Mn_{0.6}Fe_{0.4}O_3$ exhibited the highest catalytic performance with the lowest T_{50} at 379 ^{o}C.

1. Introduction

Diesel engines have been widely employed in many kinds of vehicles due to their high fuel efficiency, low CO_2 emission, and high durability. However, the soot particles emitted from these engines are threatening the environment and human health directly.[1-3] Up to now, much attention has been paid to solve this problem. Diesel particulate filter (DPF) technique is widely applied to trap the soot particles in the diesel exhaust.[4] However, excessive trapped soot particles may have a negative impact on the capture performance of DPF. Therefore, the regeneration of DPF is necessary and the removal of soot is a key problem during this process.[5, 6] An efficient solution is to burn out these soot particles trapped in DPF. Given the combustion temperature of soot particles is about 600 ^{o}C, much higher than the outlet temperature of diesel exhaust (below 400 ^{o}C), the soot cannot completely convert. Many researchers find that the oxidation catalysts deposited on the filter can reduce the combustion temperature of the soot particles, thus the soot can convert to CO_2 even at the outlet temperature.[7] The oxidation catalysts used in the diesel exhaust systems are the core part of diesel emission after treatment technology. So far, various types of catalysts have been investigated for the soot abatement, such as platinum group metal (PGM) based oxides, perovskite-type oxides, spinel-type oxides, rare earth metal oxides, and mixed transient metal oxides.[8-11] Among them, perovskite oxides receive much concern owing to their high activities, low costs, and good thermal stabilities.[12] The general chemical formula for

Catalysis Science & Technology Accepted Manuscript

perovskite oxides is ABO_3. A-site cations can be rare earth (La, Ce), alkaline (K, Na), or alkaline-earth (Ca, Sr) cations, while the B-site cations can be transition metals such as Co, Fe, Ni, Mn, or Cr. The catalytic performances of perovskite-type oxides mainly depend on the B-site ions, while affected by the A-site ions indirectly as a consequence of their catalytical inactivity.[13] Partial substitution at A-site and/or B-site will enhance the activities due to the formation of oxygen vacancies and/or the valence change of cations.[14-16] The perovskite-type oxides are regarded as the potential catalysts for soot removal.

Soot oxidation occurs on three-phase boundary between soot (solid phase), catalyst (solid phase) and gaseous reactant (gaseous phase). The contact conditions between soot and the catalysts play important roles in this kind of heterogeneous catalysis reactions.[17] The sizes of soot particles are often greater than 25 nm, much larger than the pore sizes of common catalysts (<10 nm). Therefore, these particles cannot reach the active sites on the inner surfaces of the catalysts, which leads to low catalyst utilization. An orthogonal pathway is to provide these catalysts with three-dimensionally ordered macroporous (3DOM) structure to amplify the soot combustion.[18-22] The distinct structure will indeed provide on the one hand accessible channels and enhanced mass transfer at the same time. This explains the excellent activities of the catalysts with 3DOM structure. During the past decade, many 3DOM perovskite catalysts, such as $LaFeO_3$, $LaMnO_3$, and $LaCoO_3$, have been constructed and applied in soot combustion, showing better catalytic performances than the corresponding nanoparticle ones.[19, 23-26] Among the above 3DOM perovskites, $LaMnO_3$ are easy to prepare and widely used because of the low solidification temperature of Mn.[27] Our group has found that partial introduction of Ce in 3DOM perovskite not only supports the 3DOM structure, but

Catalysis Science & Technology Accepted Manuscript

also enhances the catalytic performances.[28] Similarly, the same effects can also be achieved through the replacement of Mn by Fe, which, on this basis, can further improve the activities of perovskites.[24] However, the intrinsic activities of Mn-based perovskites for soot combustion are not so satisfactory.[29] Meanwhile, the amount of active oxygen species on the surface of perovskites are rare. Therefore, it is important to further increase the intrinsic activities and the surface active oxygen species of 3DOM Mn-based perovskite catalysts.

Alkali metals, often act as promoters, are applied broadly in various kinds of reactions.[30-32] Several studies show that alkali metals can enhance the ability of the catalysts to release active oxygen species.[33] Meanwhile, they can also form the low-melting point compounds or eutectics spontaneously, which can wet the soot surface and increase the contact between soot and catalyst.[34, 35] Among all these alkali metals, potassium with excellent reactivity is generally employed.[36-38] The combination forms between potassium and perovskite can be divided into two main types. First, potassium can be doped into the perovskite structure during the preparation process.[39] The second is that potassium can be loaded on the surface of the perovskite after it has formed.[40] However, in the first case, the macrostructure of catalysts may be destroyed due to the generation of low-melting compounds or eutectics caused by potassium.[25] Thus, we believe that it is more suitable to load potassium onto the surface rather than dope it into the lattice structure of perovskite. So far, many potassium-supported oxides have been synthesized and shown good catalytic activities for soot combustion.[41, 42] Besides, it is found that the catalytic behavior of the as-prepared catalyst is also affected by the precursor of potassium. Peralta et al. have reported that KNO_3 is better than KOH or K_2CO_3 in K/La_2O_3 towards soot combustion.[43] Therefore,

Catalysis Science & Technology Accepted Manuscript

KNO_3 supported on 3DOM perovskites are attainable.

In the present work, 3DOM perovskites $La_{0.8}Ce_{0.2}Mn_{1-x}Fe_xO_3$ ($0\leq x\leq 1$) were synthesized by colloidal crystal template method and potassium supported on 3DOM $La_{0.8}Ce_{0.2}Mn_{1-x}Fe_xO_3$ ($0\leq x\leq 1$) were prepared by incipient wetness impregnation method using KNO_3 as precursor. The techniques of XRD, FT-IR, FESEM, TEM, N_2 adsorption–desorption, XPS, H_2-TPR and O_2-TPD have been employed to characterize the physical and chemical properties of as-prepared catalysts. The catalytic performances for soot combustion were also evaluated by a temperature programmed oxidation (TPO) device. The interaction between KNO_3 and perovskite has been discussed in detail.

2. Experiment

2.1. Catalyst preparation

2.1.1 Preparation of colloidal crystal template

Monodispersed PMMA microspheres with an average diameter of 375 nm chosen as the hard temple were synthesized using emulsifier-free emulsion polymerization technique according to procedure described elsewhere.[44] The as-prepared microspheres were washed several times with deionized water and centrifuged at 3000 r/min for 10 h to form well-arranged structure. After the PMMA microspheres were fully precipitated, the supernatant was decanted and the rest solid block was dried at room temperature to obtain the colloidal crystal template.

2.1.2 Preparation of 3DOM $La_{0.8}Ce_{0.2}Mn_{1-x}Fe_xO_3$ perovskite supports

3DOM $La_{0.8}Ce_{0.2}Mn_{1-x}Fe_xO_3$ perovskites were synthesized by colloidal crystal template

Catalysis Science & Technology Accepted Manuscript

Catalysis Science & Technology Accepted Manuscript

method using PMMA as template.[45] In a typical procedure, the corresponding nitrate salts were dissolved in the mixture of ethylene glycol and methanol (40 vol%), and stirred for 2 h to form a precursor solution. The total molar concentration of the metal ions in the solution was 2 mol/L. The PMMA template was placed into the solution for about 4 h. After complete impregnation, excess solution was removed through filtration. The obtained wet samples were dried in an oven at 40 ^{o}C overnight, and calcined in a tube furnace under the air flow to remove the template. The temperature was raised to 800 ^{o}C at the rate of 1 ^{o}C/min and kept at this temperature for another 5 h.

For comparison, $La_{0.8}Ce_{0.2}Mn_{0.6}Fe_{0.4}O_3$ perovskite without macroporous structure was also prepared by the citric acid complexation method.[16] Each time, the corresponding nitrate salts were dissolved in deionized water to obtain an aqueous solution of La^{3+}, Ce^{3+}, Mn^{2+}, and Fe^{3+} with the expected stoichiometry. The molar ratio of citric acid to total metal ions was 1.1:1. The resulting solutions were evaporated to dryness at 80 °C with vigorous stirring. The clear solution gradually turned into sol and finally transformed into gel. At last, the wet gel was dried at 110 °C for 12 h and calcinated at 800 °C for 5 h.

2.1.3 Preparation of potassium supported on 3DOM $La_{0.8}Ce_{0.2}Mn_{1-x}Fe_xO_3$ catalysts

The $K/La_{0.8}Ce_{0.2}Mn_{1-x}Fe_xO_3$ catalysts were prepared by an impregnation method. Pulverized $La_{0.8}Ce_{0.2}Mn_{1-x}Fe_xO_3$ perovskites were added to an aqueous solution containing an appropriate amount of KNO_3. The mass ratio of K element to perovskite was 10 wt.% (The mass ratio of KNO_3 in the catalysts was 20.57 wt.%). Then the mixture was evaporated to dryness with vigorous stirring at 90 ^{o}C. The obtained precursors were further dried at 110 ^{o}C overnight and then calcined at 600 ^{o}C for 5 h.

2.2. Characterization

X-ray diffraction (XRD) patterns were performed with the SmartLab diffractometer (Rigaku, Japan) automated power X-ray diffraction meter operating at 100 mA and 40 kV using Cu Kα ($\lambda = 0.15418$ nm) radiation. The data of 2θ from 10 to 80 ^{o} were collected with a step scan of 0.02 ^{o}.

Brunauer-Emmett-Teller (BET) surface areas were measured by the N_2 adsorption-desorption measurement using a Micromeritics ASAP 2020 system at -196 ^{o}C. The samples were pretreated in vacuum at 300 ^{o}C for 4 h before experiments.

Fourier transform infrared (FT-IR) spectra from 400 to 1700 cm^{-1} were recorded on the Nicolet-6700 spectrometer from Thermo Electron (United States) with anhydrous KBr (Nicolet, United States) as the dispersing agent.

X-Ray fluorescence spectroscopy (XRF, Rigaku ZSX PrimusII) was used to measure the loading amount of KNO_3 on the perovskites.

Field emission scanning electron microscopy (FESEM) images were acquired with the S-4800 field-emission scanning electron microscope (Hitachi, Japan) operated at 5 kV. Transmission electron microscope (TEM) images were obtained using a JEM-2100 high-resolution transmission electron microscope (JEOL, Japan) at an accelerating voltage of 200 kV.

X-ray photoelectron spectroscopy (XPS) spectra were recorded on a PHI-5000 spectrometer using Al Kα(1486.6 eV) radiation as the excitation source. All binding energies were referenced to the C 1s peak at 284.5 eV, and Gaussian-Lorentzian and Shirley background were applied for peak analysis.

Catalysis Science & Technology Accepted Manuscript

H_2-Temperature-programmed reduction (H_2-TPR) was carried out on a chemical adsorption analyzer (Micromeritics AutoChem II 2920). 30 mg of sample (40-60 mesh) was pretreated under Ar atmosphere by calcination at 200 ^{o}C for 2 h and subsequently cooled to room temperature. Afterwards, 10% H_2/Ar flow (50 mL/min) was passed over the catalyst bed while the temperature was ramped to 850 ^{o}C at a heating rate of 10 ^{o}C/min. The alteration of H_2 concentration in the effluent was recorded online by the chemical adsorption analyzer.

O_2-Temperature-programmed desorption (O_2-TPD) was also conducted on the chemical adsorption analyzer (Micromeritics AutoChem II 2920). Each time, 30 mg of sample (40-60 mesh) was pretreated in Ar stream at 200 ^{o}C for 2 h, and then cooled down to room temperature. Then, O_2 was absorbed at 35 ^{o}C for 2 h using a gas mixture of 3% O_2/Ar, and subsequently the sample was purged by a flow of pure He stream to remove excessive and weakly adsorbed O_2. Finally, the sample was heated to 900 ^{o}C with a heating rate of 10 ^{o}C/min in a pure He flow and the desorption pattern was recorded.

2.3. Activity measurement

The catalytic activity for soot combustion under the loose contact mode was evaluated with a temperature-programmed oxidation reaction (TPO) on a fixed-bed tubular quartz reactor. Printex-U from Degussa was used as a model substance of diesel soot. Each time, 20 mg of soot and 180 mg of catalyst were carefully mixed just by spatula to obtain a loose contact. The mixture was placed in the center of a cylindrical quartz tube reactor (14 mm internal diameter) and the reaction temperature was raised from 200 ^{o}C to 700 ^{o}C with a heating rate of 2 ^{o}C/min. Reactant gas composed of 20% O_2 and 80% N_2 passed through the reactor at a flow rate of 50 mL/min. The outlet gas compositions were analyzed by an infrared

Catalysis Science & Technology Accepted Manuscript

gas analyser (Infralyt 50). In all the soot combustion experiments, the reaction lasted until the soot was completely burnt out. The values of T_{10}, T_{50} and T_{90} were defined as the temperatures when the conversion of soot reached 10%, 50% and 90%, respectively. The selectivity of CO_2 at the temperature, when the soot-burnt rate was the highest, was denoted as $S^{m}_{CO_2}$. These two factors were taken into account in the evaluation of the catalytic performances of the catalysts.

The reactivities of different O_2 species in the catalysts with soot were measured by soot-TPR. For those measurements, the catalyst-soot mixture was placed in the quartz tube and heated from 200 ^{o}C to 700 ^{o}C at a rate of 2 °C/min in N_2 flow (50 mL/min). The outlet gas compositions were analyzed by an infrared gas analyser (Infralyt 50).

3. Results and discussion

3.1. Catalysts characterization

The measurements of XRD were carried out to confirm the phase structures of 3DOM $La_{0.8}Ce_{0.2}Mn_{1-x}Fe_xO_3$ perovskites and K/$La_{0.8}Ce_{0.2}Mn_{1-x}Fe_xO_3$ catalysts ($0 \leq x \leq 1$), and the patterns are presented in Figure 1. In the Figure 1A, all the samples prepared by colloidal crystal template method exhibit highly resolved diffraction peaks, which indicates the well-developed crystalline structure has formed after high-temperature (800 ^{o}C) calcination. The $La_{0.8}Ce_{0.2}MnO_3$ perovskite exhibits diffraction peaks which are consistent with those of the rhombohedral $LaMnO_{3.15}$ (JCPDS 50-0298).[46] However, a weak peak at a value of 28 ^{o} can also be detected, suggesting that a small amount of impure phase corresponding to CeO_2 (JCPDS 34-0394) is formed after the substitution of La by Ce.[47, 48] This is because the crystal

Catalysis Science & Technology Accepted Manuscript

structure of the perovskite may distort and contract after Ce is doped into the lattice, and thus small amounts of CeO_2 may separate from perovskite. After substitution of Fe into Mn site, the intensities of the diffraction peaks are enhanced and the positions shift slightly towards lower angle with the increasing amount of Fe in the lattice, which means that a distortion from the rhombohedral structure to the orthorhombic structure has occurred. When the substitution amount reaches 1.0, the diffraction peaks of $La_{0.8}Ce_{0.2}FeO_3$ perovskite are akin to those of the orthorhombic $LaFeO_3$ (JCPDS 88-0641).[46] Meanwhile, no trace of other crystalline phases is visible after Fe is introduced, and the diffraction peaks attributed to CeO_2 still remain. As shown in Figure 1B, after K is supported on the surface of perovskites, there is no obvious change in both position and intensity of the original characteristic diffraction peaks. Besides, two new peaks appear at 23 ° and 29 °, which are ascribed to the rhombohedral KNO_3 (JCPDS 05-0377).[49, 50] However, the intensities of these two peaks are very weak owing to the extremely low content and high dispersion of KNO_3 on the surface of the perovskites. For the $K/La_{0.8}Ce_{0.2}MnO_3$ and $K/La_{0.8}Ce_{0.2}Mn_{0.8}Fe_{0.2}O_3$ catalysts, two peaks at 12 ° and 25 ° can be detected, inferring that a small amount of $K_2Mn_4O_8$ (JCPDS 16-0205) may form during the preparation.[51] With the increasing content of Fe ($y \geq 0.4$) doped into the perovskite, these diffraction peaks of $K_2Mn_4O_8$ vanish. The crystallite sizes of $La_{0.8}Ce_{0.2}Mn_{1-x}Fe_xO_3$ and $K/La_{0.8}Ce_{0.2}Mn_{1-x}Fe_xO_3$ samples are calculated by the most prominent peak using Scherrer equation and the values are shown in Table 1. For $La_{0.8}Ce_{0.2}MnO_3$ perovskite, the average crystallite size is 19.5 nm, and the values vary from 18.2 to 29.9 nm with the increasing of Fe substitution amount. After KNO_3 is deposited on the surface of 3DOM $La_{0.8}Ce_{0.2}Mn_{1-x}Fe_xO_3$ perovskites, no obvious change has been observed in their

Catalysis Science & Technology Accepted Manuscript

Catalysis Science & Technology Accepted Manuscript

crystallite sizes. Therefore, it can be concluded that the loading of KNO_3 on the surface of 3DOM $La_{0.8}Ce_{0.2}Mn_{1-x}Fe_xO_3$ perovskites has little impact on the crystalline phases, crystalline sizes and crystallinities of the 3DOM $La_{0.8}Ce_{0.2}Mn_{1-x}Fe_xO_3$ perovskites.

The FT-IR spectra of the as-prepared catalysts are displayed in Figure 2. As shown in Figure 2A, two strong vibration peaks appear around 400 and 600 cm^{-1} in all the spectra of $La_{0.8}Ce_{0.2}Mn_{1-x}Fe_xO_3$ perovskites. The peak at 400 cm^{-1} can be assigned to the bending vibration of Mn-O or Fe-O bond, and the peak at 600 cm^{-1} is related to Mn-O or Fe-O stretching in octahedral site.[29] It further proves that the perovskite has been successfully prepared using colloidal crystal template method. Meanwhile, no organic residue for PMMA has been found, which demonstrates that PMMA can be completely removed by high temperature calcination. The intensity of the absorbance peak at 600 cm^{-1} gradually decreases along with the increasing degree of Fe substitution. As depicted in Figure 2B, after the introduction of KNO_3 on the surface of 3DOM $La_{0.8}Ce_{0.2}Mn_{1-x}Fe_xO_3$ perovskites, the peaks between 400 and 600 cm^{-1} remain unchanged. It indicates that the deposition of KNO_3 on the surface of 3DOM $La_{0.8}Ce_{0.2}Mn_{1-x}Fe_xO_3$ perovskites has no effect on the perovskite structure. Meanwhile, two new signals are observed. The strong peak at 1384 cm^{-1} associates to the typical antisymmetric stretching mode of free NO_3^- ions and the other one at 825 cm^{-1} associates to the angular antisymmetric deformation of O-N-O.[52] Both of these two peaks are corresponding to KNO_3 supported on the perovskites, proving that a portion of KNO_3 remains stable in the case of K/$La_{0.8}Ce_{0.2}Mn_{1-x}Fe_xO_3$ perovskites even after calcination at 600 ^{o}C for 5 h. It is mainly due to the formation of bulk KNO_3, which is more difficult to decompose. Similar phenomenon can also be observed in literature.[51] The content of KNO_3, for example

Catalysis Science & Technology Accepted Manuscript

in 3DOM K/$La_{0.8}Ce_{0.2}Mn_{0.6}Fe_{0.4}O_3$ catalyst, is about 16.12 wt.% after calcination as revealed by XRF technique. All these results indicate that KNO_3 has been successfully dispersed on the surface of $La_{0.8}Ce_{0.2}Mn_{1-x}Fe_xO_3$ perovskites.

The BET surface areas of 3DOM $La_{0.8}Ce_{0.2}Mn_{1-x}Fe_xO_3$ perovskites and K/$La_{0.8}Ce_{0.2}Mn_{1-x}Fe_xO_3$ catalysts ($0 \leq x \leq 1$) are summarized in Table 1. It can be seen that all the surface areas of the 3DOM $La_{0.8}Ce_{0.2}Mn_{1-x}Fe_xO_3$ perovskites are larger than 15 m^2/g. Partial substitution of Fe by Mn increases the surface areas of the perovskite-type oxides, and the value reaches a maximum of 27.1 m^2/g while the content of Fe is 0.4. In the case of KNO_3-supported samples, the specific surface areas slightly decline as compared with the supports. Whereas the varying tendency of these data is basically in agreement with that of the supports. Among all the supported catalysts, K/$La_{0.8}Ce_{0.2}Mn_{0.6}Fe_{0.4}O_3$ catalyst owns the largest surface area, reaching up to 19.6 m^2/g.

Figure 3 gives the FESEM images of 3DOM $La_{0.8}Ce_{0.2}Mn_{1-x}Fe_xO_3$ perovskites ($0 \leq x \leq 1$) prepared by colloidal crystal template method and K/$La_{0.8}Ce_{0.2}Mn_{1-x}Fe_xO_3$ catalysts ($0 \leq x \leq 1$) obtained by wet impregnation method. From these images, we can find the formation of $La_{0.8}Ce_{0.2}Mn_{1-x}Fe_xO_3$ perovskites with well-defined three-dimensional ordered macroporous structure. In the three-dimensional space, the interconnected walls together with the well-ordered air spheres constitute an ‘‘inverse opal’’ structure, and the layers below are clearly visible in the FESEM images. The average diameter of the pore sizes is about 300 nm, much smaller than the particle size of the original PMMA colloidal spheres (375 nm). The decrease of pore sizes is mainly due to the shrinkage of the polymeric microspheres and the sintering of the perovskites during calcination. The thickness of the walls is 20±5 nm, similar

Catalysis Science & Technology Accepted Manuscript

to the crystallite size estimated from XRD results, which indicates that the walls are composed of crystallite grains. This special pore structure allows the soot particles to enter the inner pores of catalysts without resistance and provide more opportunities for soot particles to reach the active sites, which can accelerate the soot combustion.[25] With the loading of KNO_3, the 3DOM structure is retained. As indicated by the well consistent images of 3DOM $K/La_{0.8}Ce_{0.2}Mn_{1-x}Fe_xO_3$ catalysts and $La_{0.8}Ce_{0.2}Mn_{1-x}Fe_xO_3$ perovskites, the stirring and calcination operations in the preparation process does not lead to the collapse of macroporous structure.

In order to further study the morphologies of catalysts, especially the KNO_3 supported on the surface of 3DOM perovskites, 3DOM $La_{0.8}Ce_{0.2}Mn_{0.6}Fe_{0.4}O_3$ perovskite and $K/La_{0.8}Ce_{0.2}Mn_{0.6}Fe_{0.4}O_3$ catalyst are characterized by TEM technique and the results are shown in Figure 4. From the Figure 4a and b, it can be seen that the $La_{0.8}Ce_{0.2}Mn_{0.6}Fe_{0.4}O_3$ perovskite possesses a high-quality 3DOM structure that is composed of overlapped macropores. The pore size of 3DOM $La_{0.8}Ce_{0.2}Mn_{0.6}Fe_{0.4}O_3$ perovskite is about 300 nm, and the thickness of interconnected walls is about 20 nm. All these phenomena are in good agreement with the FESEM images. Meanwhile, the surface of the walls is smooth and has no attachment. After KNO_3 is loaded on the surface of $La_{0.8}Ce_{0.2}Mn_{0.6}Fe_{0.4}O_3$ perovskite, as shown in Figure 4c and d, there is no big change on the whole structure of the catalyst. At the same time, some dark dots in skeleton of the macropores are visible clearly, which indicates that 3DOM $La_{0.8}Ce_{0.2}Mn_{0.6}Fe_{0.4}O_3$ perovskite has been successfully decorated with well-dispersed KNO_3.

The reducibility of 3DOM $La_{0.8}Ce_{0.2}Mn_{0.6}Fe_{0.4}O_3$ perovskite and $K/La_{0.8}Ce_{0.2}Mn_{0.6}Fe_{0.4}O_3$

catalyst are investigated by H_2-TPR, as presented in Figure 5. As shown in Figure 5A, the reduction peak of $La_{0.8}Ce_{0.2}MnO_3$ shows two reduction stages. The first reduction peak α (around 350 °C) is due the reduction of Mn^{4+} to Mn^{3+}, while the second peak γ at the higher temperature is due to the reduction of Mn^{3+} to Mn^{2+}.[53] Complete reduction of Mn^{2+} to Mn^0 does not happen under the experimental conditions. The reduction step in the low region is a sign of high intrinsic oxygen reactivity, which can be regarded as the critical factor in the soot oxidation state. When Mn is partly substituted by Fe, besides the original reduction peak of Mn^{4+}, another reduction peak β appears in the region of 250-500 °C, which can be ascribed to the reduction of Fe^{4+} to Fe^{3+}.[54] Meanwhile, the peak α shifts to lower temperature, and this peak achieves the lowest temperature with further increase of Fe substitution amount to 0.4. The main reason is that certain micro-structural defects are generated around Mn sites after Fe substitution, thus promoting the diffusion through the bulk and eventually facilitating the reduction.[55] The further increasing amount of Fe substitution makes the intensity of peak α decrease and peak β increase. As shown in Figure 5B, after KNO_3 is loaded, a new peak between 300-450 °C emerges. The intensity of this peak is so strong that the original peaks referring to perovskite are almost invisible. According to the FT-IR results in Figure 2, the huge consumptions of H_2 are ascribed to the NO_3^- species stabilized in the 3DOM $K/La_{0.8}Ce_{0.2}Mn_{1-x}Fe_xO_3$.[56] It also proves that most of the alkali nitrate can still remain stable on the surface of perovskite even after 600 °C calcination. Furthermore, the reduction temperature of these NO_3^- species is also affected by the component of perovskite support, demonstrating the existence of strong interaction between KNO_3 and perovskite support. Among all the catalysts, the 3DOM $K/La_{0.8}Ce_{0.2}Mn_{0.6}Fe_{0.4}O_3$ exhibits the best reducibility

Catalysis Science & Technology Accepted Manuscript

with the lowest reduction temperature.

Soot combustion, as an oxidation reaction, usually happens on the surface of the catalysts. Therefore, the surface element compositions and surface oxygen species of the catalysts are important for this reaction. In order to get these information, XPS technique is used to investigate 3DOM $La_{0.8}Ce_{0.2}Mn_{0.6}Fe_{0.4}O_3$ perovskite and K/$La_{0.8}Ce_{0.2}Mn_{0.6}Fe_{0.4}O_3$ catalyst and the results are given in Figure 6 and 7. Figure 6 displays the La3d, Ce3d, Mn2p and Fe2p spectra of the samples. For $La_{0.8}Ce_{0.2}Mn_{0.6}Fe_{0.4}O_3$ perovskite, the La 3d5/2 doublet contained components at 837.8 and 833.6 eV are shown in Figure 6 A, which indicates that La ions are exist in the +3 oxidation state.[57] The binding energies of Fe $2p_{3/2}$ (710.4 eV) in Figure 6 D suggest that Fe cation mainly exist in the trivalent valence state.[58] The XPS spectra of Ce and Mn have been fitted by a standard Gaussian-Lorentzian deconvolution in order to further study the valence states of these two elements. As shown in Figure 6B, the bands labelled as u' and v' are ascribed to Ce^{3+} and others are assigned to Ce^{4+}. For 3DOM $La_{0.8}Ce_{0.2}Mn_{0.6}Fe_{0.4}O_3$, the molar rate of Ce^{3+} and Ce^{4+} calculated from the corresponding peak area is 0.115, which demonstrates that most of the Ce ions in the catalyst exist in the tetravalent form.[59] As shown in Figure 6C, the Mn^{4+}/Mn^{3+} in 3DOM $La_{0.8}Ce_{0.2}Mn_{0.6}Fe_{0.4}O_3$ is 0.696, which means that the trivalence is the main form of Mn ions.[60] After impregnating KNO_3 onto the surface of $La_{0.8}Ce_{0.2}Mn_{0.6}Fe_{0.4}O_3$ perovskite, the peak intensities of La 3d, Ce 3d, Mn 2p and Fe 2p drop dramatically, and the peaks can hardly be found in Figure 6. It indicates that the La, Ce, Mn and Fe atomic concentrations on the surface of the catalyst are low and KNO_3 has well covered the surface of the perovskite.

The XPS spectra of O 1s for $La_{0.8}Ce_{0.2}Mn_{0.6}Fe_{0.4}O_3$ perovskite and

Catalysis Science & Technology Accepted Manuscript

Catalysis Science & Technology Accepted Manuscript

$K/La_{0.8}Ce_{0.2}Mn_{0.6}Fe_{0.4}O_3$ catalyst are shown in Figure 7. The spectrum of $La_{0.8}Ce_{0.2}Mn_{0.6}Fe_{0.4}O_3$ has been divided into two parts using Gaussian-Lorentzian deconvolution. The peak with a lower binding energy (~528.5 eV) is assigned to the surface lattice oxygen (O_{lat}), and the other one exhibiting a higher binding energy (~530.8 eV) corresponds to the adsorbed oxygen species (O_{ads}).[39] In the case of the KNO_3-supported 3DOM $La_{0.8}Ce_{0.2}Mn_{0.6}Fe_{0.4}O_3$ catalyst, only one peak appears at 532.3 eV, which refers to the oxygen species derived from NO_3^-.[61] However, the original two kinds of O species can be hardly detected by means of XPS.

In order to further study the changes of oxygen species after the loading of KNO_3, O_2-TPD measurement was carried out and the results are displayed in Figure 8. The O_2 desorption peaks of 3DOM $La_{0.8}Ce_{0.2}Mn_{0.6}Fe_{0.4}O_3$ perovskite are relatively weak. After KNO_3 is loaded, three main O_2 desorption peaks are observed. The first peak below 200 ^oC refers to the desorption of physical adsorption oxygen species. The desorption peaks range from 200 to 400 ^oC can be assigned to the chemisorption of oxygen species. And the peak at high temperature is attributed to the lattice oxygen species from KNO_3 and perovskite.[26, 28, 62] It is obvious that the generation of the first two peaks is mainly due to the presence of K ions. As good electron donors, K ions are conducive to the adsorption and dissociation of gaseous oxygen on the surface of perovskite. Meanwhile, the presence of K ions can weaken the Fe-O or Mn-O bonds on the catalyst surface, and thus some of the lattice oxygen will convert to adsorbed oxygen.[35, 63] The increasing amount of surface adsorbed oxygen species plays an important role in accelerating the soot combustion.

3.2. Catalytic activities

Catalysis Science & Technology Accepted Manuscript

The performances of 3DOM $La_{0.8}Ce_{0.2}Mn_{1-x}Fe_xO_3$ perovskites and $K/La_{0.8}Ce_{0.2}Mn_{1-x}Fe_xO_3$ catalysts for soot combustion were evaluated by homemade TPO method and the results are illustrated in Figure 9 and Table 2. For comparison, the blank experiment without catalyst is also included, and its T_{10}, T_{50}, T_{90} and $S^{m}_{CO_2}$ are 505, 585, 640 °C and 58.3%, respectively. All the catalysts with 3DOM structure are active in soot combustion with relatively low combustion temperatures of soot and high selectivities of CO_2. For 3DOM $La_{0.8}Ce_{0.2}Mn_{1-x}Fe_xO_3$ series, the T_{50} of soot decrease by about 130 °C, and the selectivities of CO_2 exceed 98%. The substitution amount of Fe plays an important role in soot combustion. With the increasing amount of Fe content in $La_{0.8}Ce_{0.2}Mn_{1-x}Fe_xO_3$ perovskites, the catalytic performances of these perovskites experience the process of ascending first and then descending. The lowest T_{50} of soot is 448 °C when the doping amount of Fe reaches 0.4. As revealed by the above characterizations, the good performances of the Fe-doped perovskites are mainly due to the following two aspects. Firstly, the increased surface areas as the partial replacement of Mn by Fe enlarge the contact areas between the soot particles and catalysts, thus providing more active sites for soot combustion. Secondly, the introduction of Fe into the lattice of the perovskites improves the reducibilities of the catalysts, which accelerate the redox circulation during soot combustion. After KNO_3 is loaded, the CO_2 formation peaks narrow and the intensities increase compared with those of the pure perovskites. Meanwhile, the peaks shift to lower temperatures and the soot combustion temperatures decrease. Compared with perovskites, the combustion temperature of soot further decreases by about 80 °C, whereas the selectivity of CO_2 reduces slightly. It is worth mentioning that with the increasing amount of Fe, the trend in catalytic activities of

Catalysis Science & Technology Accepted Manuscript

K/$La_{0.8}Ce_{0.2}Mn_{1-x}Fe_xO_3$ series is coincident with that of $La_{0.8}Ce_{0.2}Mn_{1-x}Fe_xO_3$ series. It is noted that, $K_2Mn_4O_8$, which is found in the KNO_3 supported on perovskites with high content of Mn ($La_{0.8}Ce_{0.2}MnO_3$ and $La_{0.8}Ce_{0.2}Mn_{0.8}Fe_{0.2}O_3$), can also accelerates the soot combustion by increasing the number of active oxygen species. Similar results can be found in literatures.[51, 64] Among all the catalysts, 3DOM $La_{0.8}Ce_{0.2}Mn_{0.6}Fe_{0.4}O_3$ shows the highest catalytic activity for soot combustion, with the lowest T_{50} at 379 °C.

In order to study the effect of the 3DOM structure, $La_{0.8}Ce_{0.2}Mn_{0.6}Fe_{0.4}O_3$ and K/$La_{0.8}Ce_{0.2}Mn_{0.6}Fe_{0.4}O_3$ without macroporous structure are also prepared by citric acid complexation and the FESEM images are shown in Figure S1. These catalysts are mainly consisted of spherical primary particles. These particles condense to form agglomerates. After KNO_3 is loaded, no obvious change is observed on the morphology of catalyst. The catalytic performances of these $La_{0.8}Ce_{0.2}Mn_{0.6}Fe_{0.4}O_3$ and K/$La_{0.8}Ce_{0.2}Mn_{0.6}Fe_{0.4}O_3$ catalysts without macroporous structure are also studied and the results are shown in Figure 10. No matter whether KNO_3 is loaded or not, the particle catalysts exhibit poor catalytic activities for soot combustion compared with the 3DOM ones. With the particle $La_{0.8}Ce_{0.2}Mn_{0.6}Fe_{0.4}O_3$ or K/$La_{0.8}Ce_{0.2}Mn_{0.6}Fe_{0.4}O_3$ catalysts, the T_{50} of soot increase to 489 °C or 413 °C respectively, about 40 °C higher than the 3DOM ones. It is mainly owned to the special properties of well-ordered macropore structure. On one hand, the large pores allow soot particles to enter the inner channels of the catalysts, thus the soot can be catalyzed both on the external and internal surfaces of the 3DOM catalysts. On the other hand, the uniform macroporous network decreases the diffusional resistance when soot particles go through the 3DOM catalysts. As the improvements in soot-catalyst contact and mass transfer can both lower the soot combustion temperature, we can conclude that the catalysts with 3DOM structure are more active than the nanoparticle catalysts.[18, 20]

In order to deeply investigate the reactivity of different oxygen species during soot combustion after KNO_3 is loaded, Soot-TPR was also performed and the results are shown in Figure 11. In this process, the mixture of soot and catalyst are heated under the high purity N_2 (99.99%) atmosphere, so the soot can only be oxidized by the oxygen species, such as surface adsorbed and lattice oxygen species, existing in the catalysts, accompanied by the reduction of metallic ions.[14] As shown in Figure 11, for 3DOM $La_{0.8}Ce_{0.2}Mn_{0.6}Fe_{0.4}O_3$ (a), a weak peak corresponding to CO_2 generates between 200-350 ^oC. With the further increase of temperature, a large amount of CO_2 is formed after 400 ^oC. However, the concentration of CO is always keeping at a low level during the experiment. The generation of CO_2 at the low temperature is due to the surface adsorbed oxygen species, while the CO_2 generated at the high temperature is due to the lattice oxygen species. After the introduction of KNO_3, the CO_2 concentration at the low temperature (200-350 ^oC) increases dramatically. It demonstrates that there is an increase in the number of surface adsorbed oxygen species when KNO_3 is supported, which can accelerate soot combustion at the low temperature. With the temperature rising, the concentration of CO_2 is still higher than that of 3DOM $La_{0.8}Ce_{0.2}Mn_{0.6}Fe_{0.4}O_3$, along with the prominent increasing of CO concentration. Besides the effect of lattice oxygen species in perovskite, the soot can also be oxidized by NO_3^- species. However, the NO_3^- species trend to oxidize soot into CO rather than CO_2 in the absence of O_2, resulting in the formation of a large amount of CO. All these results are agree with those of O_2-TPD and TPO.

Based on the above results, the introduction of KNO_3 mainly plays two roles in the soot

Catalysis Science & Technology Accepted Manuscript

combustion. At the low temperature, the soot particles are directly oxidized by active oxygen species in the catalysts. The presence of K ions increases the amount of active oxygen species, which can accelerate soot combustion and lower the initiation temperature of soot. At the relatively high temperature, the soot particles are mainly oxidized by NO_3^- species rather than O_2.[56] Thereafter the formed NO_2^- after the reaction with soot can be reoxidized to NO_3^- by O_2.

$$NO_3^- + C \rightarrow NO_2^- + CO$$

$$2NO_3^- + C \rightarrow 2NO_2^- + CO_2$$

$$2NO_2^- + O_2 \rightarrow 2NO_3^-$$

$$2CO + O_2 \rightarrow 2CO_2$$

The existing NO_3^- species can continually accelerate the soot combustion through the transformation between NO_3^- and NO_2^-. However, the violent reaction may lead to the incomplete combustion of soot, thus resulting in the generation of CO and the decrease of the selectivity to CO_2.

The reusability of 3DOM K/$La_{0.8}Ce_{0.2}Mn_{0.6}Fe_{0.4}O_3$ is further examined by reusing the catalyst in soot combustion for 3 times under the same reaction conditions. As shown in Figure 12A, the profiles of CO_2 concentration as a function of reaction temperature in soot combustion are nearly the same, which means that the catalyst can be used repetitively for at least 4 times with an acceptable decrease in activity. As proved by the results of XRD, FT-IR and FESEM characterizations (Figure 12B, C and D), the morphology and crystal structure of 3DOM K/$La_{0.8}Ce_{0.2}Mn_{0.6}Fe_{0.4}O_3$ remain unchanged after used for 4 times. For comparison, the activity of 3DOM K/$La_{0.8}Ce_{0.2}Mn_{0.6}Fe_{0.4}O_3$ without calcination is also tested and the sample is reused for 3 times. As shown in Figure S2, 3DOM K/$La_{0.8}Ce_{0.2}Mn_{0.6}Fe_{0.4}O_3$ catalyst without

Catalysis Science & Technology Accepted Manuscript

calcination exhibits the same activity compared with the calcinated one, with T_{50} of soot reducing to 377 ^{o}C. However, the T_{50} of soot increases to 410 ^{o}C after recycling for 3 times. Thus we believe that the calcination process is beneficial to enhance the stability of catalysts. All these results demonstrate that the 3DOM $K/La_{0.8}Ce_{0.2}Mn_{0.6}Fe_{0.4}O_3$ calcinated at 600 ^{o}C for 5 h possesses good stability for soot combustion.

4. Conclusion

In summary, 3DOM $La_{0.8}Ce_{0.2}Mn_{1-x}Fe_xO_3$ and $K/La_{0.8}Ce_{0.2}Mn_{1-x}Fe_xO_3$ were successfully prepared and used for soot removal. The well-ordered macropore structure could enhance the contact between soot and catalysts. The strong interactions between KNO_3 and perovskite supports improved the reducibilities of catalysts and increased the amount of active oxygen species. The introduction of Fe in 3DOM $La_{0.8}Ce_{0.2}Mn_{1-x}Fe_xO_3$ series increased the intrinsic properties of catalysts. The further loading of KNO_3 dramatically lowered the soot combustion temperature from two aspects. The presence of K ions was conducive to the formation of more active oxygen species in the catalysts, which could accelerate the soot combustion at the low temperature. Meanwhile, the remained NO_3^- species oxidized the soot through redox cycle between NO_3^- and NO_2^- at the high temperature. Among all the catalysts, the 3DOM $K/La_{0.8}Ce_{0.2}Mn_{0.6}Fe_{0.4}O_3$ exhibited the highest activity and good stability for soot combustion. The catalyst can be regarded as a potential candidate for soot removal in the future.

Acknowledgements

Catalysis Science & Technology Accepted Manuscript

The work was supported by R&D Project for Environmental Protection of Jiangsu of China (NO. 2015002), the Foundation from State Key Laboratory of Materials-Oriented Chemical Engineering, Nanjing Tech University (ZK201305) and Research and Innovation Training Project for Graduate in General Universities of Jiangsu Province (No. KYZZ15_0227).

References:

1 W. Y. Lim, A. Seow, *Respirology*, 2012, **17**, 20-31.

2 R. A. Kerr, *Science*, 2013, **339**, 382.

3 R. F. Service, *Science*, 2008, **319**, 1745.

4 G. Koltsakis, O. Haralampous, C. Depcik, J. C. Ragone, *Rev. Chem. Eng.*, 2013, **29**, 1-61.

5 K. Theinnoi, S. S. Gill, A. Tsolakis, A. P. York, A. Megaritis, R. M. Harrison, *Energ. Fuel.*, 2012, **26**, 1192-1201.

6 S. Bensaid, N. Russo, *Catal. Today*, 2011, **176**, 417-423.

7 K. Mizutani, K. Takizawa, H. Shimokawa, T. Suzawa, N. Ohyama, *Top. Catal.*, 2013, **56**, 473-476.

8 A. Russell, W. S. Epling, *Catal. Rev.*, 2011, **53**, 337-423.

9 G. Zou, Y. Xu, S. Wang, M. Chen, W. Shangguan, *Catal. Sci. Technol.*, 2015, **5**, 1084-1092.

10 Y. Yu, M. Meng, F. Dai, *Nanoscale*, 2013, **5**, 904-909.

11 R. Yang, Y. Gao, J. Wang, Q. Wang, *Dalton T.*, 2014, **43**, 10317-10327.

12 A. Mishra, R. Prasad, *Catal. Rev.*, 2014, **56**, 57-81.

13 M. A. Pena, J. Fierro, *Chem. Rev.*, 2001, **101**, 1981-2018.

14 X. Guo, M. Meng, F. Dai, Q. Li, Z. Zhang, Z. Jiang, S. Zhang, Y. Huang, *Appl. Catal., B*, 2013, **142**, 278-289.

15 H. Wang, Z. Zhao, C. Xu, J. Liu, *Catal. Lett.*, 2005, **102**, 251-256.

16 S. Fang, L. Wang, Z. Sun, N. Feng, C. Shen, P. Lin, H. Wan, G. Guan, *Catal. Commun.*, 2014, **49**, 15-19.

17 J. P. Neeft, O. P. van Pruissen, M. Makkee, J. A. Moulijn, *Appl. Catal., B*, 1997, **12**, 21-31.

Catalysis Science & Technology Accepted Manuscript

18 J. Wang, G. Yang, L. Cheng, E. W. Shin, Y. Men, *Catal. Sci. Technol.*, 2015, **5**, 4594-4601.

19 M. Sadakane, T. Asanuma, J. Kubo, W. Ueda, *Chem. Mater.*, 2005, **17**, 3546-3551.

20 G. Zhang, Z. Zhao, J. Liu, G. Jiang, A. Duan, J. Zheng, S. Chen, R. Zhou, *Chem. Commun.*, 2010, **46**, 457-459.

21 Y. Wei, J. Liu, Z. Zhao, A. Duan, G. Jiang, C. Xu, J. Gao, H. He, X. Wang, *Energ. Environ. Sci.*, 2011, **4**, 2959-2970.

22 Y. Wei, Z. Zhao, X. Yu, B. Jin, J. Liu, C. Xu, A. Duan, G. Jiang, S. Ma, *Catal. Sci. Technol.*, 2013, **3**, 2958-2970.

23 J. Xu, J. Liu, Z. Zhao, J. Zheng, G. Zhang, A. Duan, G. Jiang, *Catal. Today*, 2010, **153**, 136-142.

24 J. Zheng, J. Liu, Z. Zhao, J. Xu, A. Duan, G. Jiang, *Catal. Today*, 2012, **191**, 146-153.

25 J. Xu, J. Liu, Z. Zhao, C. Xu, J. Zheng, A. Duan, G. Jiang, *J. Catal.*, 2011, **282**, 1-12.

26 Y. Wei, J. Liu, Z. Zhao, Y. Chen, C. Xu, A. Duan, G. Jiang, H. He, *Angew. Chem. Int. Edit*, 2011, **50**, 2326-2329.

27 M. Sadakane, K. Sasaki, H. Nakamura, T. Yamamoto, W. Ninomiya, W. Ueda, *Langmuir*, 2012, **28**, 17766-17770.

28 N. Feng, Y. Wu, J. Meng, C. Chen, L. Wang, H. Wan, G. Guan, *RSC Adv.*, 2015, **5**, 91609-91618.

29 H. Wang, J. Liu, Z. Zhao, Y. Wei, C. Xu, *Catal. Today*, 2012, **184**, 288-300.

30 B. Bai, J. Li, *ACS Catal.*, 2014, **4**, 2753-2762.

31 X. Tang, F. Gao, Y. Xiang, H. Yi, S. Zhao, X. Liu, Y. Li, *Ind. Eng. Chem. Res.*, 2015, **54**, 9116-9123.

32 C. F. Huo, B. S. Wu, P. Gao, Y. Yang, Y. W. Li, H. Jiao, *Angew. Chem. Int. Edit.*, 2011, **50**, 7403-7406.

33 L. Tan, G. Yang, Y. Yoneyama, Y. Kou, Y. Tan, T. Vitidsant, N. Tsubaki, *Appl. Catal., A*, 2015, **505**, 141-149.

34 V. G. Milt, M. L. Pissarello, E. E. Miró, C. A. Querini, *Appl. Catal., B*, 2003, **41**, 397-414.

35 F. E. López-Suárez, A. Bueno-López, M. J. Illán-Gómez, J. Trawczynski, *Appl. Catal., A*, 2014, **485**, 214-221.

Catalysis Science & Technology Accepted Manuscript

36 M. A. Peralta, M. S. Zanuttini, C. A. Querini, *Appl. Catal., B*, 2011, **110**, 90-98.

37 M. E. Gálvez, S. Ascaso, P. Stelmachowski, P. Legutko, A. Kotarba, R. Moliner, M. J. Lázaro, *Appl. Catal., B*, 2014, **152**, 88-98.

38 R. Matarrese, L. Castoldi, N. Artioli, E. Finocchio, G. Busca, L. Lietti, *Appl. Catal., B*, 2014, **144**, 783-791.

39 Z. Li, M. Meng, Y. Zha, F. Dai, T. Hu, Y. Xie, J. Zhang, *Appl. Catal., B*, 2012, **121**, 65-74.

40 B. Ura, J. Trawczyński, A. Kotarba, W. Bieniasz, M. J. Illan-Gomez, A. Bueno-López, F. E. López-Suárez, *Appl. Catal., B*, 2011, **101**, 169-175.

41 Y. Kim, L. Hao, J. Park, J. Miyawaki, I. Mochida, S. Yoon, *Fuel*, 2012, **94**, 516-522.

42 A. Russell, W. S. Epling, *Catal. Rev.*, 2011, **53**, 337-423.

43 M. A. Peralta, M. S. Zanuttini, M. A. Ulla, C. A. Querini, *Appl. Catal., A*, 2011, **399**, 161-171.

44 H. Arandiyan, H. Dai, K. Ji, H. Sun, J. Li, *ACS Catal.*, 2015, **5**, 1781-1793.

45 M. Sadakane, T. Asanuma, J. Kubo, W. Ueda, *Chem. Mater.*, 2005, **17**, 3546-3551.

46 N. Hosseinpour, Y. Mortazavi, A. A. Khodadadi, *Appl. Catal., A*, 2014, **487**, 26-35.

47 Q. Shen, M. Wu, H. Wang, C. He, Z. Hao, W. Wei, Y. Sun, *Catal. Sci. Technol*, 2015, **5**, 1941-1952.

48 L. Xiangwen, Z. Kebin, W. Lei, W. Baoyi, L. Yadong, *J. Am. Chem. Soc.*, 2009, **131**, 3140-3141.

49 R. Guo, Y. Hu, R. Shen, Y. Ye, L. Wu, *Chem. Eng. J.*, 2012, **211**, 31-36.

50 D. H. Kim, K. Mudiyanselage, J. Szanyi, J. C. Hanson, C. H. Peden, *J. Phys. Chem. C*, 2014, **118**, 4189-4197.

51 Q. Li, M. Meng, F. Dai, Y. Zha, Y. Xie, T. Hu, J. Zhang, *Chem. Eng. J.*, 2012, **184**, 106-112.

52 M. A. Peralta, M. S. Zanuttini, C. A. Querini, *Appl. Catal., B*, 2011, **110**, 90-98.

53 J. Chen, M. Shen, X. Wang, G. Qi, J. Wang, W. Li, *Appl. Catal., B*, 2013, **134**, 251-257.

54 X. Xiang, L. Zhao, B. Teng, J. Lang, X. Hu, T. Li, Y. Fang, M. Luo, J. Lin, *Appl. Surf. Sci.*, 2013, **276**, 328-332.

55 S. Zheng, Q. Hua, W. Gu, B. Liu, *J. Mol. Catal., A*, 2014, **391**, 7-11.

56 C. B. Grzona, I. D. Lick, E. R. Castellón, M. I. Ponzi, E. N. Ponzi, *Mater. Chem. Phys.*,

Catalysis Science & Technology Accepted Manuscript

2010, **123**, 557-562.

57 B. Feng, C. Song, G. Lv, J. Song, C. Gong, Q. Huang, *Ind. Eng. Chem. Res.*, 2011, **50**, 6660-6667.

58 K. Ji, H. Dai, J. Deng, H. Jiang, L. Zhang, H. Zhang, Y. Cao, *Chem. Eng. J.*, 2013, **214**, 262-271.

59 L. Zhang, L. Li, Y. Cao, Y. Xiong, S. Wu, J. Sun, C. Tang, F. Gao, L. Dong, *Catal. Sci. Technol.*, 2015, **5**, 2188-2196.

60 Y. Hou, M. Ding, S. Liu, S. Wu, Y. Lin, *RSC Adv.*, 2014, **4**, 5329-5338.

61 A. Yoshida, W. Shen, T. Eda, R. Watanabe, T. Ito, S. Naito, *Catal. Today*, 2012, **184**, 78-82.

62 X. Wang, Y. Zhang, Q. Li, Z. Wang, Z. Zhang, *Catal. Sci. Technol.*, 2012, **2**, 1822-1824.

63 C. A. Neyertz, E. E. Miró, C. A. Querini, *Chem. Eng. J.*, 2012, **s 181 – 182**, 93-102.

64 Y. Teraoka, K. Kanada, S. Kagawa, *Appl. Catal., B*, 2001, **34**, 73-78.

Catalysis Science & Technology Accepted Manuscript

Captions for Tables

Table 1. Crystal sizes and BET surface areas of the 3DOM $La_{0.8}Ce_{0.2}Mn_{1-x}Fe_xO_3$ and $K/La_{0.8}Ce_{0.2}Mn_{1-x}Fe_xO_3$ catalysts ($0 \leq x \leq 1$).

Table 2. The temperature and the selectivity to CO_2 for soot combustion without catalysts 3DOM $La_{0.8}Ce_{0.2}Mn_{1-x}Fe_xO_3$ and $K/La_{0.8}Ce_{0.2}Mn_{1-x}Fe_xO_3$ catalysts ($0 \leq x \leq 1$).

Catalysis Science & Technology Accepted Manuscript

Table 1. Crystal sizes and BET surface areas of the 3DOM $La_{0.8}Ce_{0.2}Mn_{1-x}Fe_xO_3$ and K/$La_{0.8}Ce_{0.2}Mn_{1-x}Fe_xO_3$ catalysts ($0 \leq x \leq 1$).

Catalyst	D^a(nm)($La_{0.8}Ce_{0.2}Mn_{1-x}Fe_xO_3$)		$S_{BET}{}^b$ (m^2g^{-1})	
	Without K	With K	Without K	With K
$La_{0.8}Ce_{0.2}MnO_3$	19.5 (32.63°)	19.6 (32.66°)	19.4	12.7
$La_{0.8}Ce_{0.2}Mn_{0.8}Fe_{0.2}O_3$	18.2 (32.62°)	18.9 (32.62°)	22.9	16.1
$La_{0.8}Ce_{0.2}Mn_{0.6}Fe_{0.4}O_3$	19.2 (32.52°)	19.2 (32.54°)	27.1	19.6
$La_{0.8}Ce_{0.2}Mn_{0.4}Fe_{0.6}O_3$	20.0 (32.50°)	20.2 (32.48°)	24.0	17.6
$La_{0.8}Ce_{0.2}Mn_{0.2}Fe_{0.8}O_3$	23.9 (32.40°)	24.0 (32.38°)	21.3	15.0
$La_{0.8}Ce_{0.2}FeO_3$	29.9 (32.24°)	30.0 (32.32°)	15.1	9.9

[a] Determined by XRD using Scherrer equation with the intensity of the most prominent peak.

[b] Surface area obtained by BET method.

Catalysis Science & Technology Accepted Manuscript

Table 2. The temperature and the selectivity to CO_2 for soot combustion without catalysts, 3DOM $La_{0.8}Ce_{0.2}Mn_{1-x}Fe_xO_3$ and K/$La_{0.8}Ce_{0.2}Mn_{1-x}Fe_xO_3$ catalysts (0≤x≤1).

Catalyst	T_{10} (°C)	T_{50} (°C)	T_{90} (°C)	$S^{m}_{CO_2}$(%)
Without Catalyst	505	585	640	58.3
$La_{0.8}Ce_{0.2}MnO_3$	387	461	531	98.1
K/$La_{0.8}Ce_{0.2}MnO_3$	335	393	456	91.7
$La_{0.8}Ce_{0.2}Mn_{0.8}Fe_{0.2}O_3$	380	455	521	99.0
K/$La_{0.8}Ce_{0.2}Mn_{0.8}Fe_{0.2}O_3$	325	384	443	91.9
$La_{0.8}Ce_{0.2}Mn_{0.6}Fe_{0.4}O_3$	372	448	513	98.3
K/$La_{0.8}Ce_{0.2}Mn_{0.6}Fe_{0.4}O_3$	322	379	429	91.9
$La_{0.8}Ce_{0.2}Mn_{0.4}Fe_{0.6}O_3$	393	464	537	98.2
K/$La_{0.8}Ce_{0.2}Mn_{0.4}Fe_{0.6}O_3$	342	399	463	91.3
$La_{0.8}Ce_{0.2}Mn_{0.2}Fe_{0.8}O_3$	398	473	541	98.8
K/$La_{0.8}Ce_{0.2}Mn_{0.2}Fe_{0.8}O_3$	358	414	482	91.8
$La_{0.8}Ce_{0.2}FeO_3$	400	477	547	98.5
K/$La_{0.8}Ce_{0.2}FeO_3$	367	424	489	92.1

Catalysis Science & Technology Accepted Manuscript

Catalysis Science & Technology Accepted Manuscript

Captions for Figures

Figure 1. XRD patterns of the 3DOM $La_{0.8}Ce_{0.2}Mn_{1-x}Fe_xO_3$ perovskites (A) and $K/La_{0.8}Ce_{0.2}Mn_{1-x}Fe_xO_3$ catalysts and pure KNO_3 (B) ($0 \le x \le 1$).

Figure 2. FT-IR spectra of the 3DOM $La_{0.8}Ce_{0.2}Mn_{1-x}Fe_xO_3$ perovskites (A) and $K/La_{0.8}Ce_{0.2}Mn_{1-x}Fe_xO_3$ catalysts (B) ($0 \le x \le 1$).

Figure 3. FESEM images of the 3DOM $La_{0.8}Ce_{0.2}Mn_{1-x}Fe_xO_3$ perovskites and $K/La_{0.8}Ce_{0.2}Mn_{1-x}Fe_xO_3$ catalysts. (a) $La_{0.8}Ce_{0.2}MnO_3$; (b) $K/La_{0.8}Ce_{0.2}MnO_3$; (c) $La_{0.8}Ce_{0.2}Mn_{0.8}Fe_{0.2}O_3$; (d) $K/La_{0.8}Ce_{0.2}Mn_{0.8}Fe_{0.2}O_3$; (e) $La_{0.8}Ce_{0.2}Mn_{0.6}Fe_{0.4}O_3$; (f) $K/La_{0.8}Ce_{0.2}Mn_{0.6}Fe_{0.4}O_3$; (g) $La_{0.8}Ce_{0.2}Mn_{0.4}Fe_{0.6}O_3$; (h) $K/La_{0.8}Ce_{0.2}Mn_{0.4}Fe_{0.6}O_3$; (i) $La_{0.8}Ce_{0.2}Mn_{0.2}Fe_{0.8}O_3$; (j) $K/La_{0.8}Ce_{0.2}Mn_{0.2}Fe_{0.8}O_3$; (k) $La_{0.8}Ce_{0.2}FeO_3$; (l) $K/La_{0.8}Ce_{0.2}FeO_3$.

Figure 4. TEM images of the 3DOM $La_{0.8}Ce_{0.2}Mn_{0.6}Fe_{0.4}O_3$ (a, b) and $K/La_{0.8}Ce_{0.2}Mn_{0.6}Fe_{0.4}O_3$ (c, d).

Figure 5. H_2-TPR profiles of the 3DOM $La_{0.8}Ce_{0.2}Mn_{1-x}Fe_xO_3$ (A) and $K/La_{0.8}Ce_{0.2}Mn_{1-x}Fe_xO_3$ catalysts (B) ($0 \le x \le 1$).

Figure 6. X-ray photoelectron spectra (XPS) of La 3d (A), Ce 3d (B), Mn 2p (C) and Fe 2d (D) regions for the 3DOM $La_{0.8}Ce_{0.2}Mn_{0.6}Fe_{0.4}O_3$ (a) and $K/La_{0.8}Ce_{0.2}Mn_{0.6}Fe_{0.4}O_3$ (b).

Figure 7. X-ray photoelectron spectra (XPS) of O 1s regions for the 3DOM $La_{0.8}Ce_{0.2}Mn_{0.6}Fe_{0.4}O_3$ (a) and $K/La_{0.8}Ce_{0.2}Mn_{0.6}Fe_{0.4}O_3$ (b).

Figure 8. O_2-TPD profiles of the 3DOM $La_{0.8}Ce_{0.2}Mn_{0.6}Fe_{0.4}O_3$ and $K/La_{0.8}Ce_{0.2}Mn_{0.6}Fe_{0.4}O_3$.

Figure 9. CO_2 concentration profiles of soot oxidation over 3DOM catalysts under loose contact conditions. (a) pure soot (without catalyst); (b) $La_{0.8}Ce_{0.2}MnO_3$; (c) $La_{0.8}Ce_{0.2}Mn_{0.8}Fe_{0.2}O_3$; (d) $La_{0.8}Ce_{0.2}Mn_{0.6}Fe_{0.4}O_3$; (e) $La_{0.8}Ce_{0.2}Mn_{0.4}Fe_{0.6}O_3$; (f)

$La_{0.8}Ce_{0.2}Mn_{0.2}Fe_{0.8}O_3$; (g) $La_{0.8}Ce_{0.2}FeO_3$; (h) K/$La_{0.8}Ce_{0.2}MnO_3$; (i) K/$La_{0.8}Ce_{0.2}Mn_{0.8}Fe_{0.2}O_3$; (j) K/$La_{0.8}Ce_{0.2}Mn_{0.6}Fe_{0.4}O_3$; (k) K/$La_{0.8}Ce_{0.2}Mn_{0.4}Fe_{0.6}O_3$; (l) K/$La_{0.8}Ce_{0.2}Mn_{0.2}Fe_{0.8}O_3$; (m) K/$La_{0.8}Ce_{0.2}FeO_3$.

Figure 10. CO_2 concentration profiles of soot oxidation over catalysts under loose contact conditions. (a) 3DOM $La_{0.8}Ce_{0.2}Mn_{0.6}Fe_{0.4}O_3$; (b) 3DOM K/$La_{0.8}Ce_{0.2}Mn_{0.6}Fe_{0.4}O_3$; (c) particle $La_{0.8}Ce_{0.2}Mn_{0.6}Fe_{0.4}O_3$; (d) particle K/$La_{0.8}Ce_{0.2}Mn_{0.6}Fe_{0.4}O_3$.

Figure 11. CO_2 and CO concentration profiles of the 3DOM $La_{0.8}Ce_{0.2}Mn_{0.6}Fe_{0.4}O_3$ (a) and K/$La_{0.8}Ce_{0.2}Mn_{0.6}Fe_{0.4}O_3$ (b) under the Soot-TPR experiment.

Figure 12. Stability test of the 3DOM K/$La_{0.8}Ce_{0.2}Mn_{0.6}Fe_{0.4}O_3$ catalyst (A), and XRD patterns (B), FT-IR spectra (C) and FESEM image (D) of the 3DOM K/$La_{0.8}Ce_{0.2}Mn_{0.6}Fe_{0.4}O_3$ catalyst and the reused catalyst.

Catalysis Science & Technology Accepted Manuscript

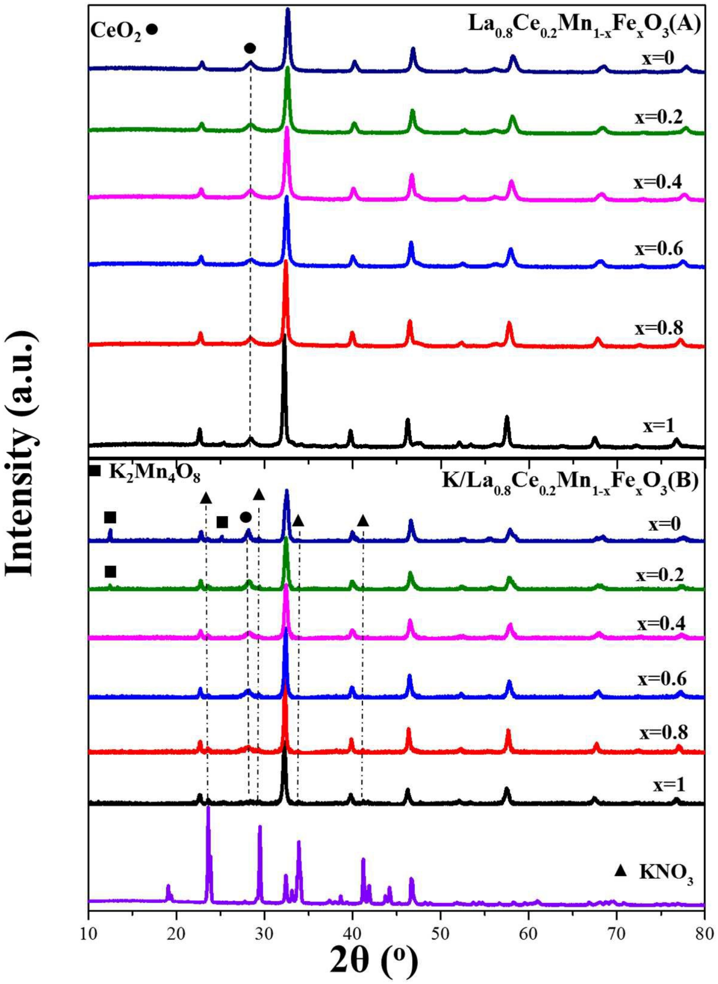

Figure 1. XRD patterns of the 3DOM $La_{0.8}Ce_{0.2}Mn_{1-x}Fe_xO_3$ perovskites (A) and $K/La_{0.8}Ce_{0.2}Mn_{1-x}Fe_xO_3$ catalysts and pure KNO_3 (B) (0≤x≤1).

Catalysis Science & Technology Accepted Manuscript

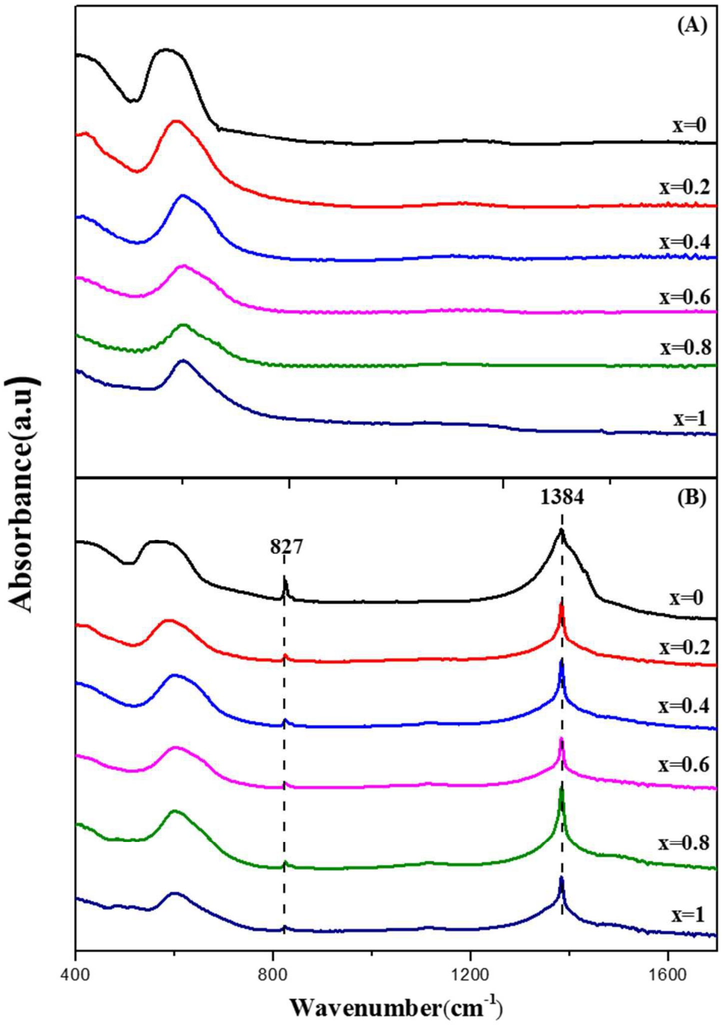

Figure 2. FT-IR spectra of the 3DOM $La_{0.8}Ce_{0.2}Mn_{1-x}Fe_xO_3$ perovskites (A) and $K/La_{0.8}Ce_{0.2}Mn_{1-x}Fe_xO_3$ catalysts (B) ($0 \leq x \leq 1$).

Catalysis Science & Technology Accepted Manuscript

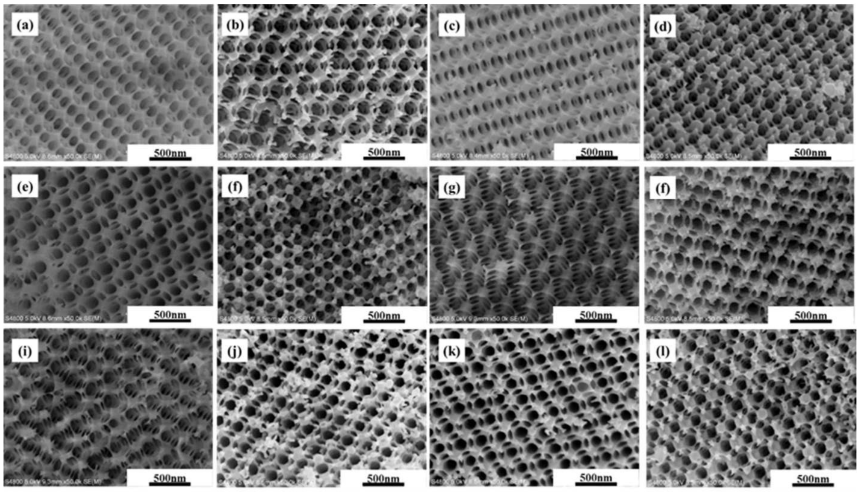

Figure 3. FESEM images of the 3DOM $La_{0.8}Ce_{0.2}Mn_{1-x}Fe_xO_3$ perovskites and $K/La_{0.8}Ce_{0.2}Mn_{1-x}Fe_xO_3$ catalysts. (a) $La_{0.8}Ce_{0.2}MnO_3$; (b) $K/La_{0.8}Ce_{0.2}MnO_3$; (c) $La_{0.8}Ce_{0.2}Mn_{0.8}Fe_{0.2}O_3$; (d) $K/La_{0.8}Ce_{0.2}Mn_{0.8}Fe_{0.2}O_3$; (e) $La_{0.8}Ce_{0.2}Mn_{0.6}Fe_{0.4}O_3$; (f) $K/La_{0.8}Ce_{0.2}Mn_{0.6}Fe_{0.4}O_3$; (g) $La_{0.8}Ce_{0.2}Mn_{0.4}Fe_{0.6}O_3$; (h) $K/La_{0.8}Ce_{0.2}Mn_{0.4}Fe_{0.6}O_3$; (i) $La_{0.8}Ce_{0.2}Mn_{0.2}Fe_{0.8}O_3$; (j) $K/La_{0.8}Ce_{0.2}Mn_{0.2}Fe_{0.8}O_3$; (k) $La_{0.8}Ce_{0.2}FeO_3$; (l) $K/La_{0.8}Ce_{0.2}FeO_3$.

Catalysis Science & Technology Accepted Manuscript

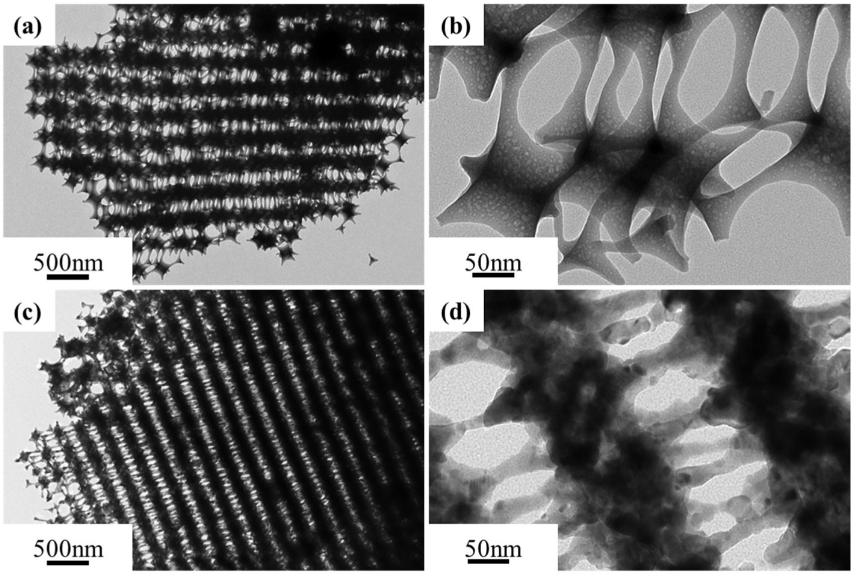

Figure 4. TEM images of the 3DOM $La_{0.8}Ce_{0.2}Mn_{0.6}Fe_{0.4}O_3$ (a, b) and $K/La_{0.8}Ce_{0.2}Mn_{0.6}Fe_{0.4}O_3$ (c, d).

Catalysis Science & Technology Accepted Manuscript

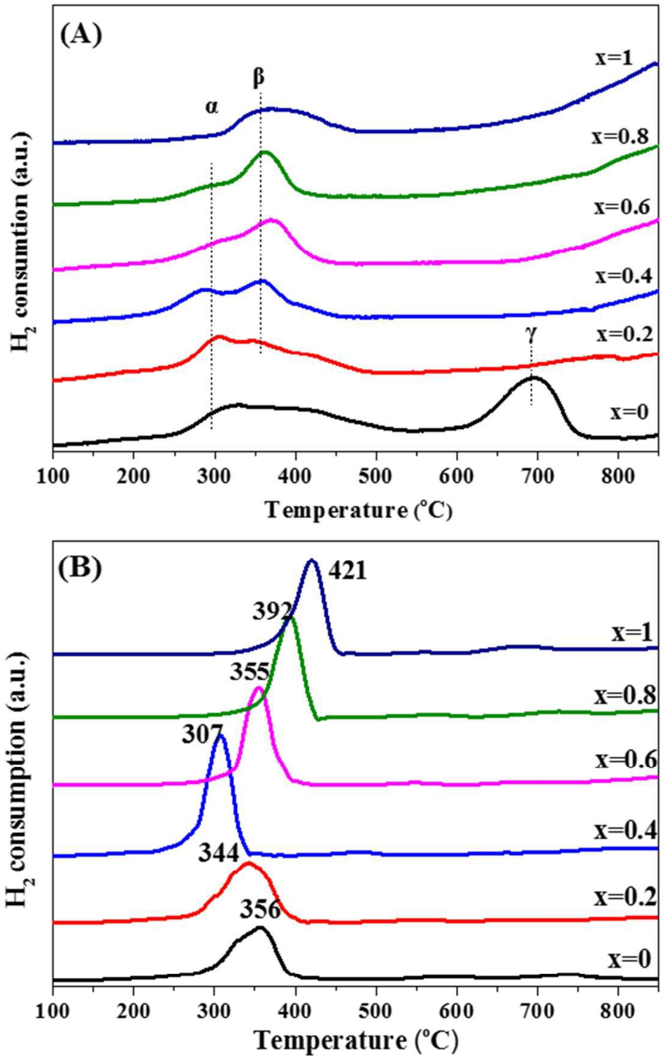

Figure 5. H_2-TPR profiles of the 3DOM $La_{0.8}Ce_{0.2}Mn_{1-x}Fe_xO_3$ (A) and K/$La_{0.8}Ce_{0.2}Mn_{1-x}Fe_xO_3$ catalysts (B) ($0 \leq x \leq 1$).

Catalysis Science & Technology Accepted Manuscript

Catalysis Science & Technology Accepted Manuscript

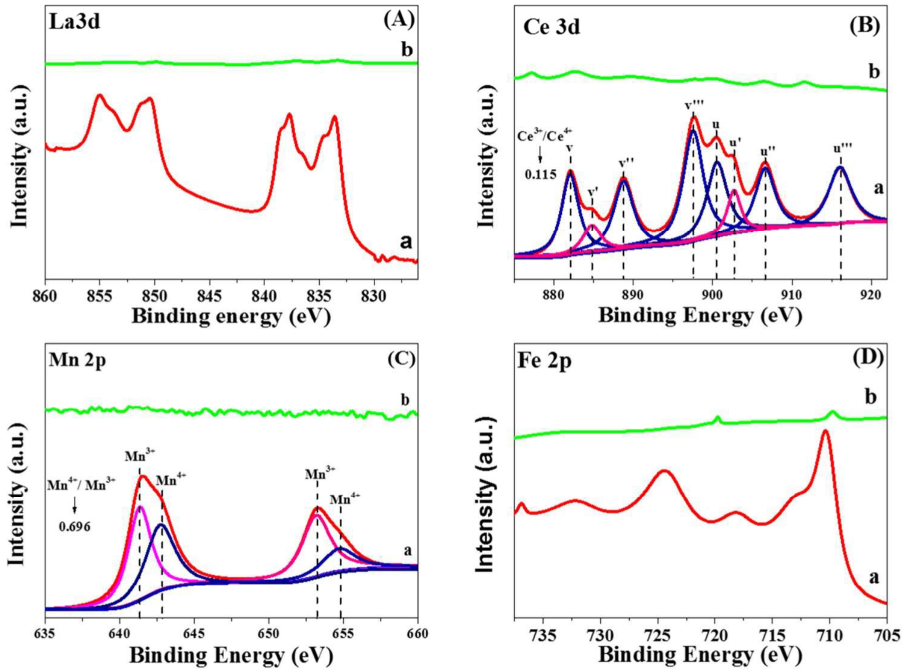

Figure 6. X-ray photoelectron spectra (XPS) of La 3d (A), Ce 3d (B), Mn 2p (C) and Fe 2d (D) regions for the 3DOM $La_{0.8}Ce_{0.2}Mn_{0.6}Fe_{0.4}O_3$ (a) and $K/La_{0.8}Ce_{0.2}Mn_{0.6}Fe_{0.4}O_3$ (b).

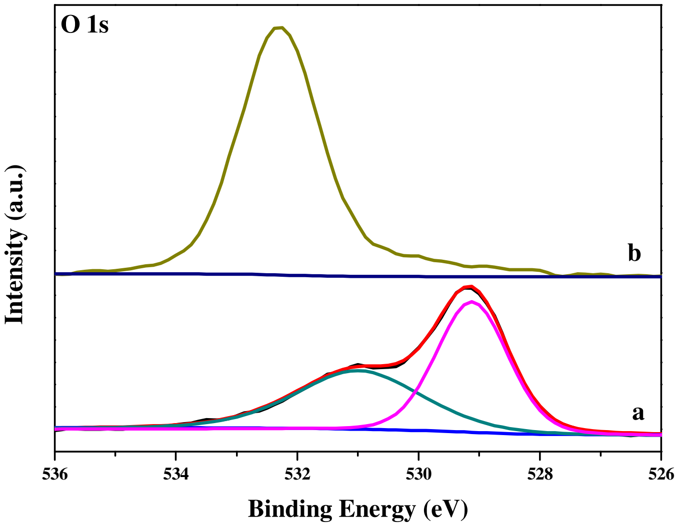

Figure 7. X-ray photoelectron spectra (XPS) of O 1s regions for the 3DOM $La_{0.8}Ce_{0.2}Mn_{0.6}Fe_{0.4}O_3$ (a) and K/$La_{0.8}Ce_{0.2}Mn_{0.6}Fe_{0.4}O_3$ (b).

Catalysis Science & Technology Accepted Manuscript

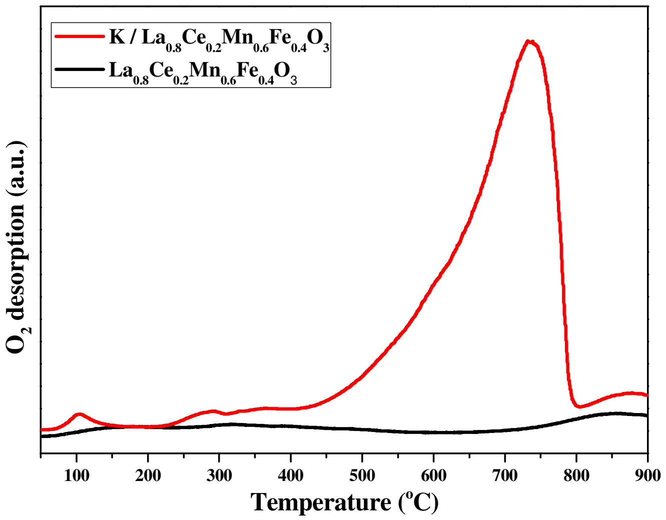

Figure 8. O_2-TPD profiles of the 3DOM $La_{0.8}Ce_{0.2}Mn_{0.6}Fe_{0.4}O_3$ and $K/La_{0.8}Ce_{0.2}Mn_{0.6}Fe_{0.4}O_3$.

Catalysis Science & Technology Accepted Manuscript

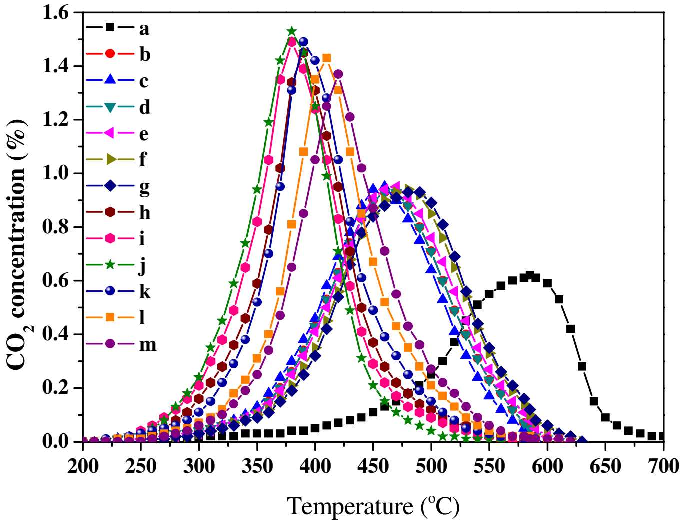

Figure 9. CO_2 concentration profiles of soot oxidation over 3DOM catalysts under loose contact conditions. (a) pure soot (without catalyst); (b) $La_{0.8}Ce_{0.2}MnO_3$; (c) $La_{0.8}Ce_{0.2}Mn_{0.8}Fe_{0.2}O_3$; (d) $La_{0.8}Ce_{0.2}Mn_{0.6}Fe_{0.4}O_3$; (e) $La_{0.8}Ce_{0.2}Mn_{0.4}Fe_{0.6}O_3$; (f) $La_{0.8}Ce_{0.2}Mn_{0.2}Fe_{0.8}O_3$; (g) $La_{0.8}Ce_{0.2}FeO_3$; (h) $K/La_{0.8}Ce_{0.2}MnO_3$; (i) $K/La_{0.8}Ce_{0.2}Mn_{0.8}Fe_{0.2}O_3$; (j) $K/La_{0.8}Ce_{0.2}Mn_{0.6}Fe_{0.4}O_3$; (k) $K/La_{0.8}Ce_{0.2}Mn_{0.4}Fe_{0.6}O_3$; (l) $K/La_{0.8}Ce_{0.2}Mn_{0.2}Fe_{0.8}O_3$; (m) $K/La_{0.8}Ce_{0.2}FeO_3$.

Catalysis Science & Technology Accepted Manuscript

Catalysis Science & Technology Accepted Manuscript

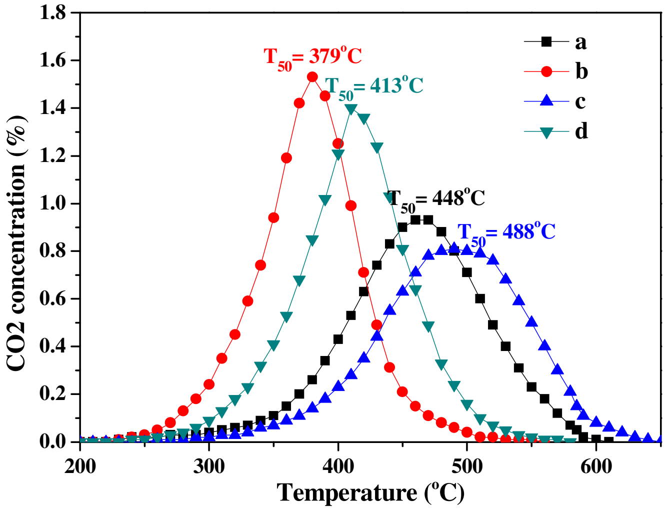

Figure 10. CO_2 concentration profiles of soot oxidation over catalysts under loose contact conditions. (a) 3DOM $La_{0.8}Ce_{0.2}Mn_{0.6}Fe_{0.4}O_3$; (b) 3DOM $K/La_{0.8}Ce_{0.2}Mn_{0.6}Fe_{0.4}O_3$; (c) particle $La_{0.8}Ce_{0.2}Mn_{0.6}Fe_{0.4}O_3$; (d) particle $K/La_{0.8}Ce_{0.2}Mn_{0.6}Fe_{0.4}O_3$.

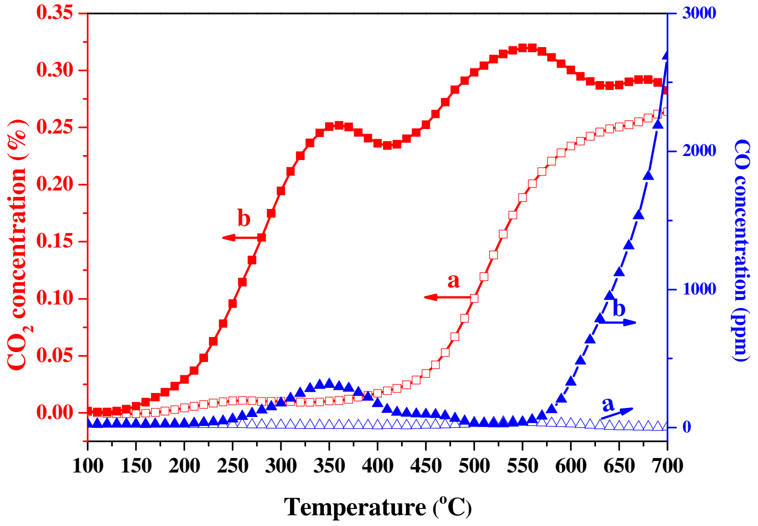

Figure 11. CO$_2$ and CO concentration profiles of the 3DOM $La_{0.8}Ce_{0.2}Mn_{0.6}Fe_{0.4}O_3$ (a) and K/$La_{0.8}Ce_{0.2}Mn_{0.6}Fe_{0.4}O_3$ (b) under the Soot-TPR experiment.

Catalysis Science & Technology Accepted Manuscript

Catalysis Science & Technology Accepted Manuscript

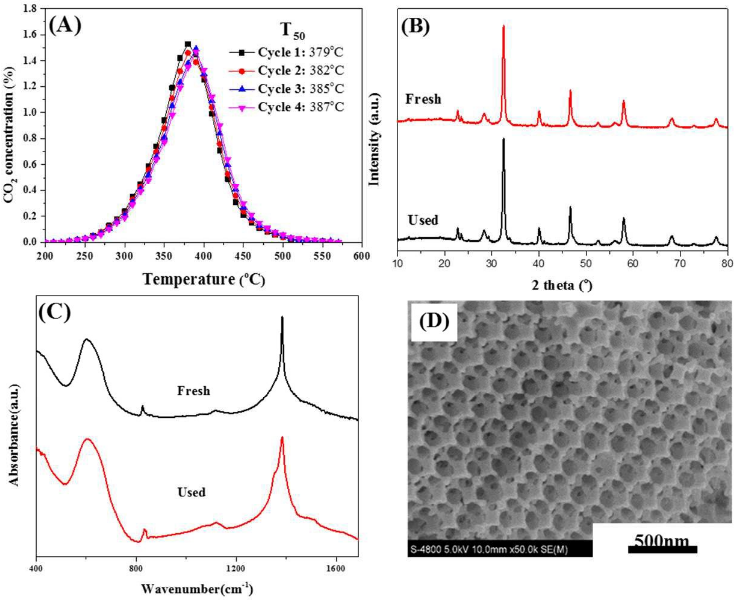

Figure 12. Stability test of the 3DOM K/$La_{0.8}Ce_{0.2}Mn_{0.6}Fe_{0.4}O_3$ catalyst (A), and XRD patterns (B), FT-IR spectra (C) and FESEM image (D) of the 3DOM K/$La_{0.8}Ce_{0.2}Mn_{0.6}Fe_{0.4}O_3$ catalyst and the reused catalyst.

Graphical Abstract

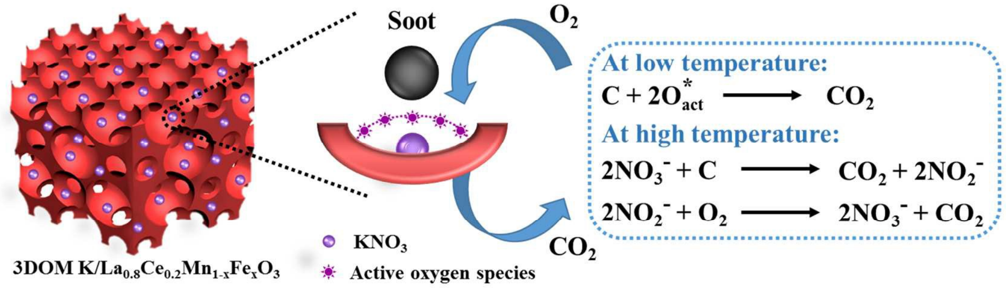

The KNO$_3$ supported on 3DOM La$_{0.8}$Ce$_{0.2}$Mn$_{1-x}$Fe$_x$O$_3$ perovskites exhibit high activities for soot combustion. The presence of potassium is conducive to the formation of more active oxygen species in the catalysts, which can accelerate the soot combustion at the low temperature. Meanwhile, the remained NO$_3^-$ species oxidize the soot through redox cycle between NO$_3^-$ and NO$_2^-$ at the high temperature.

Catalysis Science & Technology Accepted Manuscript